A dissipative particle dynamics model for studying dynamic phenomena in colloidal rod suspensions

Yawei Liu[1, a)] and Asaph Widmer-Cooper[1, 2, b)]
[1)]*ARC Centre of Excellence in Exciton Science, School of Chemistry, University of Sydney, Sydney, New South Wales 2006, Australia*
[2)]*The University of Sydney Nano Institute, University of Sydney, Sydney, New South Wales 2006, Australia*

(Dated: 30 May 2024)

A dissipative particle dynamics (DPD) model is developed and demonstrated for studying dynamics in colloidal rod suspensions. The solvent is modeled as conventional DPD particles, while individual rods are represented by a rigid linear chain consisting of overlapping solid spheres which interact with solvent particles through a hard repulsive potential. The boundary condition on the rod surface is controlled using a surface friction between the solid spheres and the solvent particles. In this work, this model is employed to study the diffusion of a single colloid in the DPD solvent, and compared with theoretical predictions. Both the translational and rotational diffusion coefficients obtained at a proper surface friction show good agreement with calculations based on the rod size defined by the hard repulsive potential. In addition, the system-size dependence of the diffusion coefficients show that the Navier-Stokes hydrodynamic interactions are correctly included in this DPD model. Comparing our results with experimental measurements of the diffusion coefficients of gold nanorods, we discuss the ability of the model to correctly describe dynamics in real nanorod suspensions. Our results provide a clear reference point from which the model could be extended to enable the study of colloid dynamics in more complex situations or for other types of particles.

I. INTRODUCTION

Colloid diffusion is a fundamental process that affects many complex, non-equilibrium phenomena in colloidal suspensions such as self-assembly[1–4] and phoretic motion[5–10]. In experiments, the diffusion of colloidal particles can be probed using light scattering techniques[11–13]. However, with the proliferation of colloidal particles of different shapes, compositions, patterns and functionalities, especially in the nanoparticle regime, interpreting the corresponding experimental data becomes more difficult, and significant limitations appear with regard to size, shape, concentration, time scale and polydispersity. On the other hand, computer simulations, due to their precise control of particle attributes and direct information about particle motion, have played a key role in interpreting experimental results and in validating theories.

Previously, we presented an overlapping-sphere model for rod-shaped colloidal particles and showed its versatility by using it within efficient dynamic simulations to characterize the phase behavior of hard-rod and rod-polymer suspensions[14]. In this work, we focus on the dynamic properties of the colloidal rods, specifically, the self-diffusion, and demonstrate that the diffusion of rod-shaped particles can also be well captured by this model, including hydrodynamic effects.

In most theoretical work and simulations, rod-shaped colloidal particles are simply modeled as a body with finite excluded volume : a hard cylinder of length L and diameter d[15–18], or a hard spherocylinder consisting of a cylindrical segment of length (L–d) and diameter d capped with two hemispheres[19–21]. However, accurately simulating rod dynamics in colloidal suspensions is still very challenging, mainly due to the difficulty of accounting for the solvent in a way that is both correct and efficient.

At the simplest level, the solvent can be taken into account through Brownian dynamics (BD)[19], in which the solvent is implicitly represented via effective frictional and random forces acting on the colloidal particles. At the same level of accuracy, implicit-solvent dynamic Monte Carlo (DMC) simulations can also be used[20,21]. Both BD and DMC simulations are computationally efficient, but require knowledge of the short-time dynamics of a single rod, obtained either from theory or experiment, to determine the friction and random forces/torques acting on the rods[19] or the elementary (translational and rotational) move size of the rods[21] in the simulations. More severely, both techniques neglect hydrodynamic interactions (HIs) from other rods mediated by the solvent, which can significantly alter dynamical correlations, especially at high volume fractions. Unfortunately, as long-ranged and multi-body interactions, HIs are difficult to treat with analytical models and usually cannot be decomposed into a pairwise sum of forces between rods.

In practice, with current computational resources, the only feasible way to consider HIs is to coarse-grain the description of the solvent[22–25]. Dissipative particle dynamics (DPD)[26,27] is one popular coarse-graining strategy, where each DPD particle represents a group of liquid molecules in which both Brownian motion and HIs can be faithfully reproduced. The DPD method can be viewed as an extension of standard molecular dynamics (MD), and thus is very easy to implement using existing MD codes.

The original DPD method of Hoogerbrugge and Koelman[28] was designed to model the colloidal particle as a rigid body of many "frozen" DPD particles suspended in a fluid composed of free DPD particles. However, this type of DPD colloid particle has a poorly defined surface due to the soft interaction, and the

[a)]yawei.liu@sydney.edu.au
[b)]asaph.widmer-cooper@sydney.edu.au

interaction between the colloid and the liquid is also difficult to map onto simple theoretical models since it depends on the detailed structure of the constituent particles in the colloid. Here, inspired by the idea in Ref. 29, we use a core-shell model in which the spheres constituting the rod are represented as a hard core, which the liquid particle cannot penetrate, surrounded by a friction shell, in which the liquid particles interact with the sphere via additional friction and random forces. As a result, the colloidal rod has a clearly defined size and the liquid-solid boundary condition can be easily tuned.

As a first step, the present work focuses on the self-diffusion of a single rod in the DPD liquid. Nevertheless, the HIs between rods can still be investigated in our simulations via the system-size effect.

The paper is organized as follows: In Sec. II, we briefly review the continuum theory for the diffusion coefficient of rod-shaped colloidal particles and discuss corrections due to the system-size effect. We introduce our model and simulation method in Sec. III and present the simulation results and a comparison with theoretical predictions in Sec. IV. A brief summary of the key results is given in Sec. V.

II. THEORY

A. Continuum theory for diffusion of rod-shaped particles

In order to compare our simulation results with theory, we use relations that allow calculation of the theoretical diffusion coefficients based on the particle size. In 1979 and 1980, Tirado and García de la Torre[17,18] derived the equations to calculate the diffusion coefficient of a cylindrical particle of length L and diameter d in a liquid under the stick boundary condition (BC) in the framework of continuum theory. In the theory, the translational diffusion coefficients for motion along the longitudinal and transverse dimensions ($D_\parallel$ and $D_\perp$), and for the motion in a random direction (D_t) can be expressed as

$$D_\parallel = k_B T(\ln p + \nu_\parallel)/(2\pi\eta L), \tag{1}$$
$$D_\perp = k_B T(\ln p + \nu_\perp)/(4\pi\eta L), \tag{2}$$
$$D_t = k_B T(\ln p + \nu_t)/(3\pi\eta L), \tag{3}$$

where k_B is the Boltzmann constant, T is the temperature, η is the dynamic viscosity of the liquid, and p is the aspect ratio with $p = L/D$. Meanwhile, the rotational diffusion coefficient for the orientation of the long axis (D_r) can be written as

$$D_r = 3k_B T(\ln p + \nu_r)/(\pi\eta L^3). \tag{4}$$

In Eqs. 1–4, $\nu_\parallel$, $\nu_\perp$, ν_t and ν_r are the so-called end-effect corrections, which are functions of p, and are given by

$$\begin{aligned}
\nu_\parallel &= -0.207 + 0.980/p - 0.133/p^2,\\
\nu_\perp &= 0.839 + 0.185/p + 0.233/p^2,\\
\nu_t &= 0.312 + 0.565/p - 0.1/p^2,\\
\nu_r &= -0.662 + 0.917/p - 0.05/p^2.
\end{aligned} \tag{5}$$

This theory has been used as a fundamental tool to analyze diffusion processes in experimental and computational studies[30–39], and has been argued to be applicable to rod-shaped particles with, approximately, $2 < p < 30$[40].

B. System-size dependence

The continuum theory of Tirado and García de la Torre gives the translational/rotational diffusion coefficient of a rod-shaped particle far from any other particles or boundaries. Our simulations are performed using boxes with periodic boundary conditions (PBC), and the HIs between the colloidal particle and its periodic images can cause significant system-size effects on the diffusion coefficients.

For a single spherical particle in a cubic periodic box with edge length L_{box}, i.e., assuming that the particle and its periodic images are arranged in a simple cubic array, the corrected translational diffusion coefficient can be written in terms of an expansion of the volume fraction $\phi = \pi d^3/(6L_{box}^3)$[41–43],

$$D_{t,PBC} = \begin{cases} D_{t,0}Q & \text{stick,} \\ D_{t,0}QQ' & \text{slip.} \end{cases} \tag{6}$$

where $Q = \left(1 - 1.7601\phi^{1/3} + \phi - 1.5593\phi^2\right)$ and $Q' = (3 + A\phi)/2$ with $A = 27.9 \pm 0.4$. Here, $D_{t,0}$ is the diffusion coefficient in an infinitely large box for the stick BC, which is given by the well-known Stokes-Einstein (SE) relation[44,45]

$$D_t^{SE,stick} = k_B T/(3\pi\eta d), \tag{7}$$

with d the diameter of the spherical particle. Note that Eq. 6 can also lead to the SE relation for the slip BC at $\phi \to 0$, i.e., $D_t^{SE,slip} = k_B T/(2\pi\eta d)$.

Analogously, the corrected rotational diffusion coefficient can be expressed as[46]

$$D_{r,PBC} = D_{r,0}(1 - \phi), \tag{8}$$

where $D_{r,0}$ is the rotational diffusion coefficient with no system-size effect. For spherical particles with a stick BC, $D_{r,0}$ is given by the Stokes-Einstein-Debye (SED) relation[47]

$$D_r^{SED} = k_B T/(\pi\eta d^3). \tag{9}$$

In order to apply the same corrections to rod-shaped particles, we treat the rod as a sphere which has the same diffusion coefficient. The diameter of the equivalent sphere (i.e. the effective diameter $\overline{d}$) can be obtained by rewriting Eqs. 3 and 4 into the same forms as Eqs. 7 and 9, and are given by the

$$\begin{aligned}
\overline{d}_t &= L/(\ln p + \nu_t),\\
\overline{d}_r &= L/\sqrt[3]{3(\ln p + \nu_r)}.
\end{aligned} \tag{10}$$

for the translational diffusion and the rotational diffusion, respectively. Consequently, we expect that the system-size effect on the diffusion coefficient of rod-shaped particles is also given by Eqs. 6 and 8 with $\phi = \overline{\phi} = \pi\overline{d}^3/(6L_{box}^3)$, $D_{t,0} = D_t$ in Eq. 3, and $D_{r,0} = D_r$ in Eq. 4.

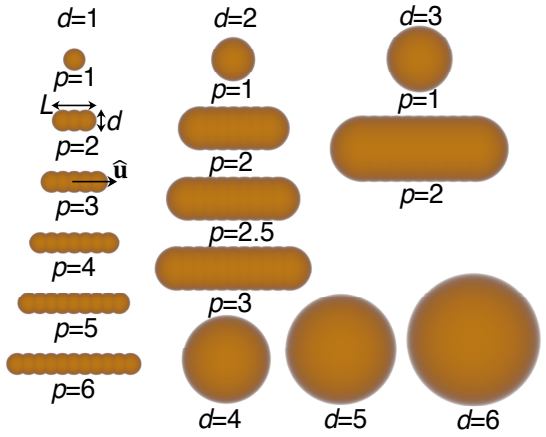

FIG. 1. Schematic illustration of all colloidal particles used in this work. The colloidal spheres of diameter d are represented by a single solid sphere of the same diameter, while the colloidal rods of diameter d and aspect ratio $p = L/d$ are modeled as a rigid body made up of several overlapping solid spheres of the same diameter. For the rods, the distance between consecutive solid spheres is fixed at $\Delta l = 0.5$, and the direction of the long axis is indicated by the unit vector $\hat{\mathbf{u}}$.

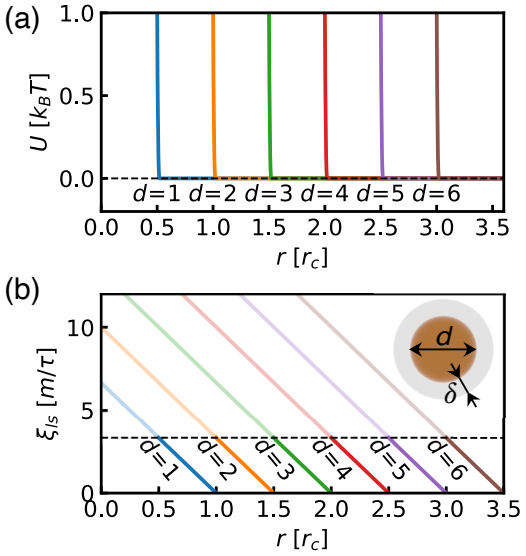

FIG. 2. Interactions between a solid sphere of diameter d and a liquid particle: (a) Modified Mie potential (Eq. 12) at different values d. (b) The surface friction coefficient (ξ_{ls}) in Eq. 13 as a function of the center-to-center distance at $\gamma_{ls,0} = 10$ for various values of d. For all lines, the solid parts represent the results in the friction shell (i.e. $d/2 < r < d/2 + \delta$) while the transparent parts are the results in the "hard" core (i.e. $r < d/2$). Inset: Schematic illustration of the core-shell model for the solid sphere, which is represented by a central hard core of diameter d surrounded by a friction shell of thickness δ.

III. MODEL AND METHOD

A. Model for colloids and solvent

In our model, the liquid is explicitly modeled as dissipative particle dynamics (DPD) particles each with the mass m. All DPD particles interact with each other via a conservative force $\mathbf{F}^C_{ij}$, a dissipative force $\mathbf{F}^D_{ij}$ and a random force $\mathbf{F}^R_{ij}$ given by

$$\begin{aligned}
\mathbf{F}^C_{ij} &= a(1 - r_{ij}/r_c)\hat{\mathbf{r}}_{ij} && r_{ij} < r_c \\
\mathbf{F}^D_{ij} &= -\gamma(1 - r_{ij}/r_c)^2(\hat{\mathbf{r}}_{ij} \cdot \mathbf{v}_{ij})\hat{\mathbf{r}}_{ij} && r_{ij} < r_c \\
\mathbf{F}^R_{ij} &= \sqrt{2k_BT\gamma}(1 - r_{ij}/r_c)\theta_{ij}\Delta t^{-1/2}\hat{\mathbf{r}}_{ij} && r_{ij} < r_c
\end{aligned} \tag{11}$$

between beads i and j. Here, $r_{ij} = |r_{ij}|$ is the centre-to-centre distance between two particles i and j, $\hat{\mathbf{r}}_{ij} = \mathbf{r}_{ij}/r_{ij}$ is the unit vector pointing between the two beads, and γ is the dissipative constant, $\mathbf{v}_{ij}$ is the vector difference in velocities between the two beads, θ_{ij} is a Gaussian white noise variable with $\theta_{ij} = \theta_{ji}$, and Δt is the simulation time step. All these three forces vanish when $r_{ij} \geq r_c$ with r_c the cut-off distance. Hereafter, all quantities are reported in their reduced units with r_c as the length unit, k_BT as the energy unit, m as the mass unit, $\tau = r_c\sqrt{m/(k_BT)}$ as the time unit.

The rod-shaped colloids are described as pseudo-hard spherocylinders with total length L and diameter d. In our model, these spherocylinders are represented by the model we developed previously for studying phase behavior in rod and rod-polymer suspensions[14]: individual rods are represented by a rigid linear chain consisting of overlapping solid spheres of diameter d with their centers distributed uniformly on a line segment of length $(L-d)$ (see Fig. 1 for examples).

The solid spheres have two interactions with the DPD liquid particles: (i) a hard-core interaction to prevent liquid particles penetrating the sphere; and (ii) an effective interaction due to the surface friction to control the liquid-solid boundary condition[48]. In our model, the hard-core interaction is replaced by a continuous pseudo-hard-core potential in the form of a modified Mie potential with exponents (50, 49), i.e.,

$$U(r_{ij}) = 50\left(\frac{50}{49}\right)^{49}\varepsilon\left[\left(\frac{\sigma}{r_{ij}-\Delta}\right)^{50} - \left(\frac{\sigma}{r_{ij}-\Delta}\right)^{49}\right] + \varepsilon \tag{12}$$

truncated at $r_{cut} = (50/49)\sigma + \Delta$. Here, ε is the interaction energy, σ is the interaction distance with $\sigma = 1$, Δ is the shifted distance with $\Delta = d/2 - 1$. This modified Mie(50, 49) potential can remain the same shape for spheres with different sizes [see Fig. 2 (a)]. In addition, we set the rod density equal to that of the liquid, i.e. $\rho_r = \rho_l$, and therefore the mass of each rod sphere is $m_r = \rho_l V/N$ with the rod volume $V = \pi d^2[d + 1.5(L - d)]/6$.

The sphere/solvent friction is modeled as a piar dissipative force which directly depends on the relative velocity between the solid sphere and the liquid particle ($\mathbf{v}_{ij}$)[48], i.e,

$$\begin{aligned}
\mathbf{F}^F_{ij} &= -\xi_{ls}(r_{ij})\mathbf{v}_{ij} \\
&= -\gamma_{ls}(1 - \frac{r_{ij}}{d/2+\delta})\mathbf{v}_{ij} \\
&= -\gamma_{ls,0}\frac{d/2+\delta}{\delta}(1 - \frac{r_{ij}}{d/2+\delta})\mathbf{v}_{ij} \quad r_{ij} < d/2 + \delta
\end{aligned} \tag{13}$$

Here, ξ_{ls} is the surface friction coefficient, and γ_{ls} is the

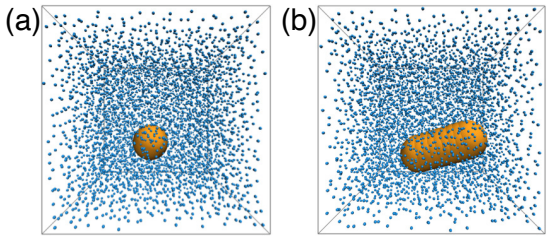

FIG. 3. Two typical simulation boxes used in this work. Each box contains one colloidal sphere (a) or one colloidal rod (b) in the liquid. Colloidal particles are orange while the liquid particles are blue.

friction constant, which is an adjustable parameter that characterizes the strength of the surface friction and can be used to vary the slip length. The position-dependent function $\xi_{ls}(r_{ij})$ is a monotonically decreasing function of the distance, and vanishes at a cutoff $(d/2+\delta)$ to mimic the finite range of the surface interaction. As a result, this force acts in a friction shell of thickness δ around the sphere [see inset in Fig. 2 (b)]. Note that γ_{ls} is corrected for spheres with different sizes by the multiplier $(d/2+\delta)/\delta$ so that ξ always has the same values in the friction shell [see Fig. 2 (b)]. Additionally, a stochastic force obeying the fluctuation-dissipation theorem is required to ensure the correct equilibrium statistics, i.e.,

$$\mathbf{F}^S_{ij} = \sqrt{2k_BT\xi_{ls}(r_{ij})}\theta_{ij}\Delta t^{-1/2}\cdot \mathbf{v}_{ij}/v_{ij}, \qquad (14)$$

with $v_{ij} = |\mathbf{v}_{ij}|$.

Note that the core-shell model described above differs slightly from our previous one[14] as well as the one in Whittle *et al.*'s work[29]. The latter two models use the same friction force in the shell as the dissipative term in the original DPD model (Eq. 11), which implies that when a DPD liquid particle passes all the way through the friction shell of the solid sphere, the friction disappears unless there is a radial component to the velocity[49,50], which leads to poor control of the boundary condition on the solid surface.

B. Simulation method

Figure. 3 shows two examples of the simulation boxes used to investigate the diffusion of colloidal particles in this work. Each box is cubic and contains one colloidal sphere or rod and many liquid particles. Periodic boundary conditions were applied in all directions. The box size was varied to investigate the system-size effect on the simulation results, and the number of liquid particles was chosen so that the bulk liquid density was $\rho_l = 3$. All simulations were carried out using the parallel software package LAMMPS[51] in an isochoric, isothermal (NVT) ensemble with the dimensionless temperature $k_BT/\varepsilon = 1$. The velocity-Verlet algorithm was used to integrate the equations of motion with a time step $\Delta t = 0.005$. All simulations were performed with $\gamma = 100$, $a = 25$ for the DPD forces (Eq. 11) and $\delta = 0.5$ for the friction force (Eq. 13).

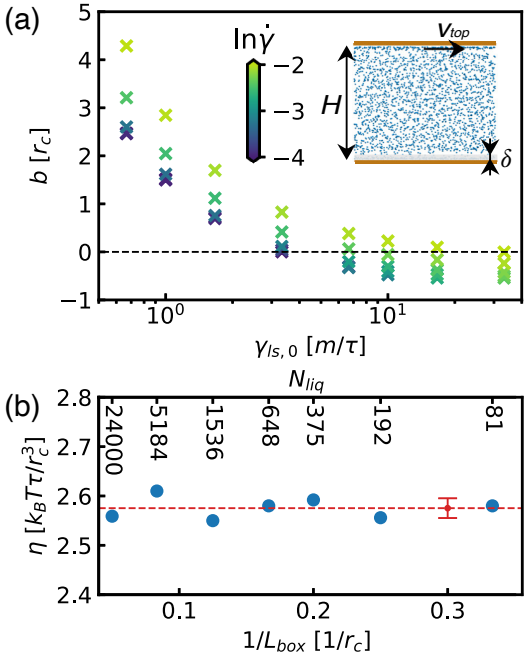

FIG. 4. (a) Relation between the slip length b and the surface friction parameter $\gamma_{ls,0}$ at different apparent shear rates $\dot{\gamma} = v_{top}/H$. Inset: Simulation box used to determine b. A stick boundary condition can be implemented at $\gamma_{ls,0} \approx 10/3$. (b) Shear viscosity η of the DPD liquid as a function of the inverse box length $1/L_{box}$ (bottom scale) for $N = 81 - 24000$ liquid particles (top scale). The horizontal dash line indicates the average value (2.57) and the corresponding standard deviation (±0.02).

C. Slip and stick boundary conditions

The slip BC is implemented with no surface friction (i.e., $\gamma_{ls,0} = 0$). For the stick BC, we determined the appropriate $\gamma_{ls,0}$ by measuring the slip length on a flat wall in a cubic simulation box with edges $L_{box} = 8$ (see insert in Fig. 4). There is a bottom wall at $z(x,y) = 0$ and a top wall at $z(x,y) = H = L_{box}$. Both walls were fixed, and interact with the liquid particles via the terms described in Eq. 12 with $\Delta = -1$ and in Eqs. 13 and 14. Here, r_{ij} is the distance between the liquid particle and the wall in the z direction. A Couette flow is produced by imposing a constant force in the x-direction on all liquid particles with $z > H-2$. The top wall is a slip one with $\gamma_{ls,0} \equiv 0$. The slip length b on the bottom wall for a given $\gamma_{ls,0}$ is defined as the extrapolation length of the velocity profile, i.e., the distance from the wall at which the liquid velocity equals 0. We changed the magnitude of the force imposed on the liquid particles to obtain the values of b at different apparent shear rates $\dot{\gamma} = v_{top}/H$ with v_{top} the liquid velocity near the top wall. As shown in Fig. 4 (a), when the apparent shear rate is small enough, the slip length b does not change significantly with $\dot{\gamma}$, and we conclude that the stick BC can be implemented on a flat solid surface by using $\gamma_{ls,0} \sim 10/3$. Because the slip length can be smaller on a curved solid surface[52–54], which also appears to be the case with our model (see Fig. S1 in the

supplementary material), several values of $\gamma_{ls,0} \geq 10/3$ were tried for the case of the stick BC in our simulations.

D. Determining the viscosity of the liquid

The shear viscosity of the liquid (η) is calculated using the Green-Kubo formula[55] in simulations with a box consisting of pure DPD liquid. We performed the simulation at various system sizes with 81-24000 liquid particles, using runs with duration of $10^5\tau$, and obtained $\eta = 2.57 \pm 0.02$ [see Fig. 4 (b)]. No significant system-size dependence on the shear viscosity exists in our model, which is consistent with previous studies for Lennard-Jones fluids and TIP3P water[42,56].

E. Determining the diffusion coefficient of colloidal particles

The translational diffusion coefficient can be evaluated from the mean-square displacement (MSD) of the colloidal particle using the following equations

$$\begin{aligned} \langle \Delta r_{\parallel}^2(t) \rangle &= \langle |(\mathbf{r}(t_0+t) - \mathbf{r}(t_0)) \cdot \hat{\mathbf{u}}(t_0)|^2 \rangle = 2D_{\parallel} t, \\ \langle \Delta r_{\perp}^2(t) \rangle &= \langle |(\mathbf{r}(t_0+t) - \mathbf{r}(t_0)) \times \hat{\mathbf{u}}(t_0)|^2 \rangle = 4D_{\perp} t, \\ \langle \Delta r^2(t) \rangle &= \langle |\mathbf{r}(t_0+t) - \mathbf{r}(t_0)|^2 \rangle = 6D_t t, \end{aligned} \tag{15}$$

where $\mathbf{r}$ is the position of the center of mass of the colloidal particle, $\hat{\mathbf{u}}$ is a unit vector along the long axis of the rod (see Fig. 1), t is the time, t_0 is the reference time, and the brackets $\langle \dots \rangle$ indicate averaging over all t_0.

Analogously, the rotational diffusion is quantified through the *rotational* mean-square displacement (RMSD) during time interval t as follows

$$\langle \Delta \vec{\varphi}^2(t) \rangle = \langle |\vec{\varphi}(t_0+t) - \vec{\varphi}(t_0)|^2 \rangle = 4D_r t. \tag{16}$$

Here, $\vec{\varphi}(t) = \int_0^t \Delta\vec{\varphi}(t')dt'$ with $\Delta\vec{\varphi}(t')$ a vector with direction given by $\hat{\mathbf{u}}(t) \times \hat{\mathbf{u}}(t+t')$ and with magnitude given by $\cos^{-1}[\hat{\mathbf{u}}(t) \cdot \hat{\mathbf{u}}(t+t')]$ during the time interval t'. With this definition, RMSD is unbounded and the diffusion coefficient can be evaluated in a large time range[57,58].

Moreover, in order to obtain better statistics, rather than using a single long trajectory, we gather a large number of short trajectories for each colloidal particle (at least 200) with a duration of 1000τ and only use data from the last 500τ of each for the calculations. This means that the MSD/RMSD in Eqs. 15 and 16 are also averaged over all these independent trajectories. Figure S2 in the supplementary material shows some examples of the linear fitting of the MSD/RMSD used to determine the corresponding diffusion coefficients.

IV. RESULTS AND DISCUSSIONS

A. Colloidal spheres

As a test of our model, we first studied the diffusion of spherical colloids with $d = 1-6$ (see Fig. 1 for the spheres and

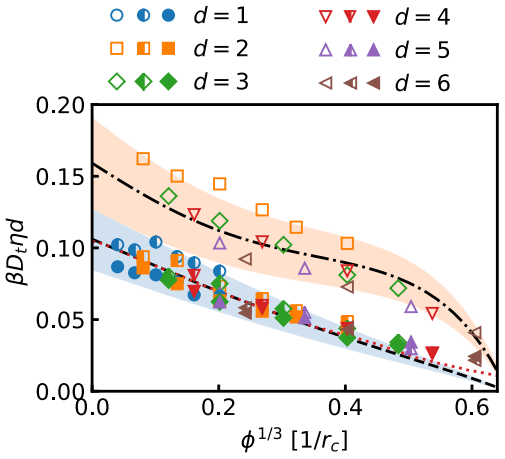

FIG. 5. Dimensionless translational diffusion coefficient ($\widetilde{D}_t = \beta D_t \eta d$) for colloidal spheres with various values of d obtained from the simulations with different box sizes [characterized by the volume fraction $\phi = \pi d^3/(6L_{box}^3)$] at $\gamma_{ls,0} = 0$ (empty symbols), $\gamma_{ls,0} = 10/3$ (half-filled symbols) and $\gamma_{ls,0} = 20/3$ (solid symbols). The dash-dot (dash) line represents the results of continuum theory at slip (stick) BC obtained from Eq. 6 and 7. The colored bands show values within ±20% of the theoretical predictions.

Table S1 in the supplementary material for the corresponding simulation boxes). Figure 5 shows the dimensionless translational diffusion coefficient ($\widetilde{D}_t = \beta D_t \eta d$ with $\beta = 1/k_B T$) obtained from simulations with different box sizes under slip BC (i.e. $\gamma_{ls,0} = 0$) and stick BC (i.e. $\gamma_{ls,0} = 10/3$ and $20/3$). The corresponding results calculated from the continuum theory (Eqs. 6 and 7) are also plotted.

Firstly, we find good agreement between the simulation results and theoretical values. Only for the smallest sphere with $d = 1$ and the slip BC are the simulation results ($\widetilde{D}_t \sim 0.33$ for $\phi^{1/3} < 0.2$) much larger than the theoretical predictions. This indicates that as the colloid approaches the size of the DPD solvent, the drag force from the solvent is substantially reduced compared to the theoretical predictions. This colloid-size effect becomes weak for larger colloids, but can still be observed at the slip BC as a systematic decrease in D_t as d increases. In the case of the stick BC, simulation results of $\widetilde{D}_t$ do not significantly depend on the sphere size, implying that the colloid-size effect is more important for the form drag due to the pressure field (i.e. the overall drag at the slip BC) than for the friction drag due to the shear stress field (i.e. the major drag at the stick BC).

Secondly, the theoretical $\widetilde{D}_t$ at the stick BC can be well reproduced in the simulations when a surface friction of $\gamma_{ls,0} = 10/3 - 20/3$ is imposed between the solid and the solvent (also see Fig. S3 in the supplementary material for $\widetilde{D}_t$ at larger $\gamma_{ls,0}$). This range of $\gamma_{ls,0}$ is only slightly larger than the appropriate value for a flat solid surface [see Fig. 4 (a)], indicating that the stick BC does not break down even for the smallest spheres in our model. However, even at $\gamma_{ls,0} = 20/3$, we do not observe a strict stick BC on the solid surface from the velocity profile around a solid sphere (see Fig. S1), and the excellent match

between the simulation results and theoretical values may be caused differences between the bulk viscosity and the local "microviscosity" experienced by the colloidal particles[59].

Thirdly, the system-size effect on $\widetilde{D}_t$ described by Eq. 6 is also well described by our model over the range of volume fraction that we considered with only some small discrepancies in the presence of stick BC at large volume fractions. There are a couple of important points to note here. The first is that Eq. 6 clearly breaks down at high volume fractions: it predicts $D_t = 0$ around $\phi^{1/3} \sim 0.65$ (i.e. $\phi \sim 0.27$), which is well below the lowest solid densities ($\phi \sim 0.52$ and 0.56 for simple cubic packing and random loose packing, respectively). This breakdown is because Eq. 6 does not consider lubrication or quadrupolar effects which become important at short range[43]. It is therefore logical for our model to deviate from Eq. 6 at higher volume fractions. The second point is that our simulations depart from Eq. 6 near $\phi^{1/3} \sim 0.4$. This is close to the critical volume fraction for colloids in a simple cubic lattice separated by a surface-to-surface distance of $3r_c$ (i.e. $\phi^{1/3} = 0.32 - 0.54$ for $d = 2 - 6$). This distance is approximately twice the thickness of the interface region (i.e. $1.0 - 1.5r_c$, see Fig. S1 in the supplementary material), implying that the non-uniform solvent near the colloids may be starting to affect the HIs. This means that for $\phi 1/3 > 0.4$, the applicability of any model is likely to depend on whether it provides a reasonable description of the solvent structure near the colloids.

Note that in our model the single colloidal sphere represented by a mass point has no angular momentum, so the corresponding rotational diffusion coefficient cannot be obtained.

B. Colloidal rods

We then studied the diffusion of the rod-shaped colloids shown in Fig. 1 in different sized boxes (see Table S1 in the supplementary material) using either slip BC (i.e. $\gamma_{ls,0} = 0$) or stick BC (i.e. $\gamma_{ls,0} = 10/3$ and $20/3$). Figure 6 shows the dimensionless translational and rotational diffusion coefficients ($\widetilde{D}_t = \beta D_t \eta \overline{d}_t$ and $\widetilde{D}_r = \beta D_t \eta \overline{d}_r^3$), obtained from simulations and from continuum theory (see Table S2 in the supplementary material for the effective diameters), as a function of the effective volume fraction ($\overline{\phi}_t$ and $\overline{\phi}_r$). Note that the theoretical calculations based on Eqs. 1-5 are only valid for the stick BC.

For $\widetilde{D}_t$, we also see good agreement between the simulation results and theoretical values (±20%) when $\overline{\phi}_t^{1/3} < 0.3$ at both $\gamma_{ls,0} = 10/3$ and $20/3$. These results indicate that: i) theoretical predictions of $\widetilde{D}_t$ for colloidal rods can be reproduced by our model faithfully at the stick BC; ii) the system-size effect can be well described by treating these short rods as equivalent spheres with the same diffusion coefficients at relative low volume fractions (i.e. $\overline{\phi}_t^{1/3} < 0.3$), and the Navier-Stokes HIs between these colloidal rods are correctly included in our model. Note that the discrepancies at $\overline{\phi}_t^{1/3} > 0.3$ may be not entirely caused by the non-uniform solvent around the rods. The maximum packing density of rods is higher than that of spheres, which means that the diffusion constant should deviate more strongly from the continuum scaling than in the sphere case. Thus, it is difficult to exactly determine the consistent region between our model and the continuum theory, but at least for $\overline{\phi}_t^{1/3} < 0.4$, our model still shows reasonable results compared to the the theoretical calculations.

For the case of the slip BC, $\widetilde{D}_t$ for rods with $d \geq 2$ appear to lie on a single curve as a function of $\overline{\phi}_t$, suggesting a universal relationship for the system-size effect at the slip BC. Our simulation results give a linear relationship with $D_t = (-1.04\overline{\phi}_t^{1/3} + 1.10) D_t^{SE,slip}$. For small rods with $d = 1$, the strong colloid-size effect causes the universal relationship

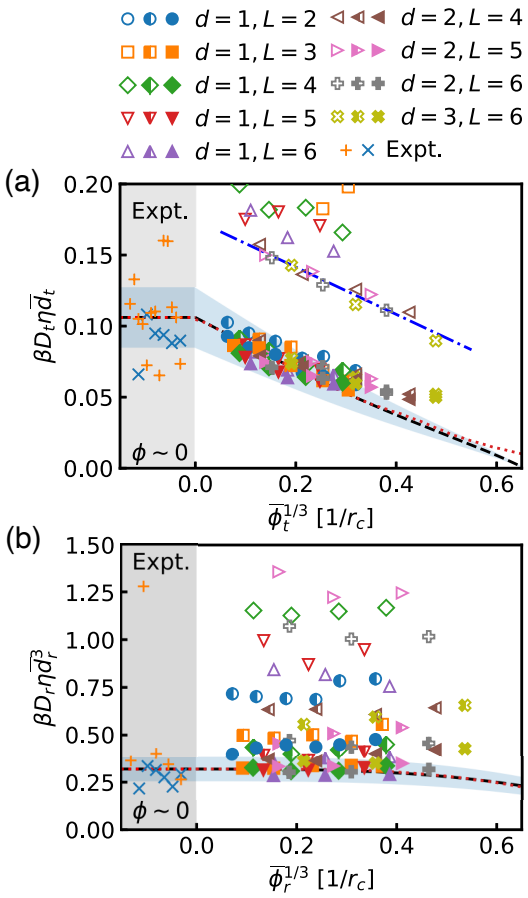

FIG. 6. Dimensionless (a) translational and (b) rotational diffusion coefficient (i.e. $\widetilde{D}_t = \beta D_t \eta \overline{d}_t$ and $\widetilde{D}_r = \beta D_t \eta \overline{d}_r^3$) for colloidal rods with various values of d obtained from simulations with different box sizes [characterized by the effective volume fraction $\overline{\phi} = \pi \overline{d}^3/(6L_{box}^3)$] at $\gamma_{ls,0} = 0$ (empty symbols), $\gamma_{ls,0} = 10/3$ (half-filled symbols) and $\gamma_{ls,0} = 20/3$ (solid symbols). The dash line represents the results of continuum theory at stick BC obtained from Eqs. 1-10. The colored bands show values within ±20% of the theoretical predictions. The red dash-dot line in (a) shows a linear fit to $\widetilde{D}_t$ of colloidal rods with $d \geq 2$ that have the slip BC. The experimental diffusion coefficients for gold nanorods from Ref. 31 by Rodriguez-Fernandez *et al.* (cross symbols) and Ref. 39 by Nixon-Luke *et al.* (plus symbols) are plotted in the grey region.

to break down.

Moreover, the ratios between D_t along the longitudinal and transverse dimensions ($D_\parallel/D_\perp$) obtained from simulations with the stick BC show considerable scatter, but still cluster around the expected trend *vs.* L/d (see Fig. S4 in the supplementary material).

For $\widetilde{D}_r$, we find that the simulation results with $\gamma_{ls,0} = 10/3$ are larger than the theoretical values with the stick BC, especially for small and short rods (e.g. $d = 1$, $L = 2$; $d = 2$, $L = 4$ and $d = 3$, $L = 6$). This is attributed to the fact that in our overlapping-sphere model for rods, the velocity at the ends is simply represented by the center-of-mass velocity of the end spheres, and thus the friction-drag on a rotating rod is artificially reduced. Such artificial end-effects are less important for long rods (e.g. $d = 1$ and $L = 6$), and can be offset by increasing the surface friction between the solid spheres and the solvent particles. For example, when $\gamma_{ls,0} = 20/3$, we obtain better agreement between the simulation results and theoretical values. Moreover, the system-size effect on $\widetilde{D}_r$ at the stick BC also exists in the simulations, and agrees with the theoretical prediction at sufficiently small volume fractions (i.e. $\overline{\phi}_r^{1/3} < 0.4$). Therefore, both the translational and rotational diffusion of colloidal rods as described by the continuum theory can be faithfully reproduced by our model at $\gamma_{ls,0} = 20/3$, which is comparable to $\gamma_{ls,0} = 10/3$ for the stick BC on a flat solid surface.

In Fig. 6, we also plot experimental results for the diffusion coefficients of gold nanorods in dilute aqueous solutions from Ref. 31 by Rodriguez-Fernandez *et al.* and Ref. 39 by Nixon-Luke *et al.*. When converting these results into dimensionless units, we have taken a 4 nm thick double-layer of CTAB (i.e. cetyltrimethylammonium bromide) around the rods to calculate the effective rod length and diameter. The same idea was employed in Ref. 5 where a $10 - 15$ nm thick PVP (i.e. poly-vinylpyrrolidone) layer was included in the effective rod dimensions in order to obtain reasonable agreement with the continuum theory. We can see that better agreement between the experimental and the calculated values can be achieved for most experimental results when the gold core plus the CTAB bilayer are treated as a whole rigid body and a stick BC is applied. This is especially clear for the smaller rods studied in Ref. 31 (see Fig. S5 in the supplementary material for the comparison without CTAB bilayer corrections).

We note, however, that there is not universal agreement on how the CTAB bilayer affects the effective dimensions of the rods. In Ref. 34, Michael Glidden *et al.* claimed that including the CTAB bilayer in the effective nanorod size is unnecessary or even incorrect in their analysis. The appropriate thickness of the CTAB bilayer is also unclear: Rodriguez-Fernandez *et al.* used a value of 4 nm in their analysis, while in Ref. 35, the authors used a value of 2 nm to obtain the best match between theoretical predictions and the measured data; and both of these two values differ from the thickness measured in another experiment (i.e., $3.0 - 3.4$ nm)[60]. One possible explanation for this inconsistency is that the morphology of the bilayer depends on the CTAB concentration and varies from paper to paper.

In the nanoscale regime, many factors that influence the diffusion coefficient (such as breakdown of the stick BC, variations of local "microviscosity" experienced by the colloids, and changes in hydrodynamic size in different environments) could be present in any given case, and it is difficult to figure out the exact causes of small departures from the continuum theory. Considering these uncertainties, we find that the continuum theory applies fairly well for nanorods when some reasonable corrections are taken into account. Thus, our DPD model, which can well reproduce the diffusion behavior of colloidal rods described by the continuum theory in dilute solutions, should be a useful tool for studying the dynamics of rod-shaped nanoparticles, including phenomena such as self-assembly and phoretic transport.

V. CONCLUSIONS

In this work, we have developed a coarse-grained model for colloidal rod suspensions based on the dissipative particle dynamics (DPD) method: while the solvent is explicitly represented by conventional DPD particles, the colloidal rods are modeled as a rigid chain of overlapping solid spheres that interact with the solvent particles via a hard repulsive potential. In addition, a surface friction is employed to control the boundary condition at the rod/solvent interface. Diffusion coefficients obtained using this model, for both colloidal spheres and rods, were compared with continuum theory.

Both the translational diffusion coefficient for colloidal spheres and the translational/rotational diffusion coefficients obtained for rods show good agreement with theoretical calculations based on the size defined by the hard repulsive potential at the slip/stick boundary. The results show the same dependence on system size as predicted by the continuum theory for volume fractions where $\phi^{1/3} < 0.4$, showing that the Navier-Stokes hydrodynamic interactions are also correctly included in the model in this concentration range. At higher concentrations, our model shows a logical departure from the continuum theory, with its accuracy likely to depend on how well it accounts for non-uniformities in the solvent structure around the colloid.

Many experiments show that the diffusion of gold nanorods in dilute solutions can be well described by continuum theory as long as a reasonable correction to their effective hydrodynamic sizes is considered based on the thickness of the ligand layer around them. Thus, our model should be applicable to the study of other dynamic phenomena in such nanorod suspensions.

Compared to implicit-solvent methods such as BD[19] and DMC simulations[21], our model with explicit solvent particles is more computationally expensive, but it has a clear advantage for solving some problems in which hydrodynamics must be taken into account. For example, for the colloidal transport driven by an electric field (i.e. electrophoresis) or a solute concentration gradient (i.e. diffusiophoresis)[61], treating solvent dynamics explicitly is necessary to obtain the correct colloidal dynamics[62]. On the other hand, compared to explicit-solvent models with other coarse-graining strategies, such as the lattice Boltzmann (LB) method[63], stochastic rotation dy-

namics (SRD)[22], and Fluid Particle Dynamics (FPD)[64], the DPD model naturally describes Brownian dynamics and is readily extended to more complex system such as charged suspensions. For example, we have recently used our DPD model to study the oriented assembly of charged gold nanorods in the presence of an electric field[10].

More generally, the current work provides a clear starting point from which the model could be extended to explore the solution dynamics of other colloidal particles (e.g. Janus rods[37] or helical rods[65]) and in more complex situations (e.g. in more concentrated suspensions[66] or in confined spaces[67]).

SUPPLEMENTARY MATERIAL

See supplementary material for velocity profiles around a colloidal sphere in a flow field, determining the diffusion coefficient from the MSD/RMSD, size of simulation boxes, effective diameter of colloidal rods, translational diffusion coefficients of colloidal spheres at larger surface frictions, ratio of translational diffusion coefficient along the longitudinal and transverse dimensions, and comparison between experimental diffusion coefficients of nanorods and theoretical predictions without CTAB bilayer corrections.

ACKNOWLEDGMENTS

This work was supported by the Australian Research Council under Grant CE170100026. Computational resources were provided by the University of Sydney HPC service, and the Pawsey Supercomputing Centre with funding from the Australian Government and the Government of Western Australia.

DATA AVAILABILITY STATEMENT

The data that support the findings of this study are available from the corresponding author upon reasonable request.

[1] V. J. Anderson and H. N. W. Lekkerkerker, "Insights into phase transition kinetics from colloid science," Nature **416**, 811–815 (2002).
[2] Y. Wang, Y. Wang, D. R. Breed, V. N. Manoharan, L. Feng, A. D. Hollingsworth, M. Weck, and D. J. Pine, "Colloids with valence and specific directional bonding," Nature **491**, 51–55 (2012).
[3] S. Whitelam and R. L. Jack, "The Statistical Mechanics of Dynamic Pathways to Self-Assembly," Annu. Rev. Phys. Chem. **66**, 143–163 (2015).
[4] M. A. Boles, M. Engel, and D. V. Talapin, "Self-Assembly of Colloidal Nanocrystals: From Intricate Structures to Functional Materials," Chem. Rev. **116**, 11220–11289 (2016).
[5] B. M. Van Der Zande, J. K. Dhont, M. R. Böhmer, and A. P. Philipse, "Colloidal dispersions of gold rods characterized by dynamic light scattering and electrophoresis," Langmuir **16**, 459–464 (2000).
[6] W. Ahmed, E. S. Kooij, A. Van Silfhout, and B. Poelsema, "Quantitative analysis of gold nanorod alignment after electric field-assisted deposition," Nano Lett. **9**, 3786–3794 (2009).
[7] A. Singh, N. J. English, and K. M. Ryan, "Highly ordered nanorod assemblies extending over device scale areas and in controlled multilayers by electrophoretic deposition," J. Phys. Chem. B **117**, 1608–1615 (2013).
[8] Z. Tan, M. Yang, and M. Ripoll, "Anisotropic thermophoresis," Soft Matter **13**, 7283–7291 (2017).
[9] Z. Wang, D. Niether, J. Buitenhuis, Y. Liu, P. R. Lang, J. K. G. Dhont, and S. Wiegand, "Thermophoresis of a Colloidal Rod: Contributions of Charge and Grafted Polymers," Langmuir **35**, 1000–1007 (2019).
[10] H. Zhang, Y. Liu, M. F. S. Shahidan, C. Kinnear, F. Maasoumi, J. Cadusch, E. M. Akinoglu, T. D. James, A. Widmer-Cooper, A. Roberts, and P. Mulvaney, "Direct Assembly of Vertically Oriented, Gold Nanorod Arrays," Adv. Funct. Mater. **30**, 2006753 (2020).
[11] B. J. Berne and R. Pecora, *Dynamic light scattering: with applications to chemistry, biology, and physics* (Courier Corporation, 2000).
[12] D. Lehner, H. Lindner, and O. Glatter, "Determination of the Translational and Rotational Diffusion Coefficients of Rodlike Particles Using Depolarized Dynamic Light Scattering," Langmuir **16**, 1689–1695 (2000).
[13] R. Cerbino and V. Trappe, "Differential Dynamic Microscopy: Probing Wave Vector Dependent Dynamics with a Microscope," Phys. Rev. Lett. **100**, 188102 (2008).
[14] Y. Liu and A. Widmer-Cooper, "A versatile simulation method for studying phase behavior and dynamics in colloidal rod and rod-polymer suspensions," J. Chem. Phys. **150**, 244508 (2019).
[15] S. Broersma, "Rotational Diffusion Constant of a Cylindrical Particle," J. Chem. Phys. **32**, 1626–1631 (1960).
[16] S. Broersma, "Viscous Force Constant for a Closed Cylinder," J. Chem. Phys. **32**, 1632–1635 (1960).
[17] M. M. Tirado and J. G. de la Torre, "Translational friction coefficients of rigid, symmetric top macromolecules. Application to circular cylinders," J. Chem. Phys. **71**, 2581–2587 (1979).
[18] M. M. Tirado and J. G. de la Torre, "Rotational dynamics of rigid, symmetric top macromolecules. Application to circular cylinders," J. Chem. Phys. **73**, 1986–1993 (1980).
[19] H. Löwen, "Brownian dynamics of hard spherocylinders," Phys. Rev. E **50**, 1232–1242 (1994).
[20] A. Patti and A. Cuetos, "Brownian dynamics and dynamic Monte Carlo simulations of isotropic and liquid crystal phases of anisotropic colloidal particles: A comparative study," Phys. Rev. E **86**, 011403 (2012).
[21] A. Cuetos and A. Patti, "Equivalence of Brownian dynamics and dynamic Monte Carlo simulations in multicomponent colloidal suspensions," Phys. Rev. E **92**, 022302 (2015).
[22] J. T. Padding and A. A. Louis, "Hydrodynamic interactions and Brownian forces in colloidal suspensions: Coarse-graining over time and length scales," Phys. Rev. E **74**, 031402 (2006).
[23] I. Pagonabarraga, B. Rotenberg, and D. Frenkel, "Recent advances in the modelling and simulation of electrokinetic effects: bridging the gap between atomistic and macroscopic descriptions," Phys. Chem. Chem. Phys. **12**, 9566 (2010).
[24] D. S. Bolintineanu, G. S. Grest, J. B. Lechman, F. Pierce, S. J. Plimpton, and P. R. Schunk, "Particle dynamics modeling methods for colloid suspensions," Comput. Part. Mech. **1**, 321–356 (2014).
[25] U. D. Schiller, T. Krüger, and O. Henrich, "Mesoscopic modelling and simulation of soft matter," Soft Matter **14**, 9–26 (2018).
[26] R. D. Groot and P. B. Warren, "Dissipative particle dynamics: Bridging the gap between atomistic and mesoscopic simulation," J. Chem. Phys. **107**, 4423–4435 (1997).
[27] P. Español and P. B. Warren, "Perspective: Dissipative particle dynamics," J. Chem. Phys. **146**, 150901 (2017).
[28] P. J. Hoogerbrugge and J. M. V. A. Koelman, "Simulating Microscopic Hydrodynamic Phenomena with Dissipative Particle Dynamics," Europhys. Lett. **19**, 155–160 (1992).
[29] M. Whittle and K. P. Travis, "Dynamic simulations of colloids by core-modified dissipative particle dynamics," J. Chem. Phys. **132**, 124906 (2010).
[30] H. Maeda and Y. Maeda, "Direct Observation of Brownian Dynamics of Hard Colloidal Nanorods," Nano Lett. **7**, 3329–3335 (2007).
[31] J. Rodríguez-Fernández, J. Pérez-Juste, L. M. Liz-Marzán, and P. R. Lang, "Dynamic light scattering of short au rods with low aspect ratios," J. Phys. Chem. C **111**, 5020–5025 (2007).
[32] S. L. Eichmann, B. Smith, G. Meric, D. H. Fairbrother, and M. A. Bevan, "Imaging Carbon Nanotube Interactions, Diffusion, and Stability in Nanopores," ACS Nano **5**, 5909–5919 (2011).
[33] A. Günther, P. Bender, A. Tschöpe, and R. Birringer, "Rotational diffusion of magnetic nickel nanorods in colloidal dispersions," J. Phys. Condens. Matter **23**, 325103 (2011).

[34] M. Glidden and M. Muschol, "Characterizing Gold Nanorods in Solution Using Depolarized Dynamic Light Scattering," J. Phys. Chem. C **116**, 8128–8137 (2012).

[35] P. Zijlstra, M. Van Stee, N. Verhart, Z. Gu, and M. Orrit, "Rotational diffusion and alignment of short gold nanorods in an external electric field," Phys. Chem. Chem. Phys. **14**, 4584–4588 (2012).

[36] B.-Y. Cao and R.-Y. Dong, "Molecular dynamics calculation of rotational diffusion coefficient of a carbon nanotube in fluid," J. Chem. Phys **140**, 34703 (2014).

[37] A. Kharazmi and N. V. Priezjev, "Molecular Dynamics Simulations of the Rotational and Translational Diffusion of a Janus Rod-Shaped Nanoparticle," J. Phys. Chem. B **121**, 7133–7139 (2017).

[38] R. Nixon-Luke and G. Bryant, "A Depolarized Dynamic Light Scattering Method to Calculate Translational and Rotational Diffusion Coefficients of Nanorods," Part. Part. Syst. Charact. **36**, 1800388 (2019).

[39] R. Nixon-Luke and G. Bryant, "Differential dynamic microscopy to measure the translational diffusion coefficient of nanorods," J. Phys. Condens. Matter **32**, 115102 (2020).

[40] M. M. Tirado, C. L. Martínez, and J. G. de la Torre, "Comparison of theories for the translational and rotational diffusion coefficients of rod-like macromolecules. Application to short DNA fragments," J. Chem. Phys. **81**, 2047–2052 (1984).

[41] H. Hasimoto, "On the periodic fundamental solutions of the Stokes equations and their application to viscous flow past a cubic array of spheres," J. Fluid Mech. **5**, 317 (1959).

[42] I.-C. Yeh and G. Hummer, "System-Size Dependence of Diffusion Coefficients and Viscosities from Molecular Dynamics Simulations with Periodic Boundary Conditions," J. Phys. Chem. B **108**, 15873–15879 (2004).

[43] K. Ichiki, A. E. Kobryn, and A. Kovalenko, "Targeting transport properties in nanofluidics: Hydrodynamic interaction among slip surface nanoparticles in solution," J. Comput. Theor. Nanosci. **5**, 2004–2021 (2008).

[44] W. Sutherland, "LXXV. A dynamical theory of diffusion for non-electrolytes and the molecular mass of albumin," London, Edinburgh, Dublin Philos. Mag. J. Sci. **9**, 781–785 (1905).

[45] J. C. M. Li and P. Chang, "Self-Diffusion Coefficient and Viscosity in Liquids," J. Chem. Phys. **23**, 518–520 (1955).

[46] M. Linke, J. Köfinger, and G. Hummer, "Rotational Diffusion Depends on Box Size in Molecular Dynamics Simulations," J. Phys. Chem. Lett. **9**, 2874–2878 (2018).

[47] G. H. Koenderink, H. Zhang, D. G. A. L. Aarts, M. P. Lettinga, A. P. Philipse, and G. Nägele, "On the validity of Stokes–Einstein–Debye relations for rotational diffusion in colloidal suspensions," Faraday Discuss. **123**, 335–354 (2003).

[48] J. Zhou, J. Smiatek, E. S. Asmolov, O. I. Vinogradova, and F. Schmid, "Application of Tunable-Slip Boundary Conditions in Particle-Based Simulations," in *High Perform. Comput. Sci. Eng. '14*, edited by W. E. Nagel, D. H. Kröner, and M. M. Resch (Springer International Publishing, 2015) pp. 19–30.

[49] P. Español, "Fluid particle dynamics: A synthesis of dissipative particle dynamics and smoothed particle dynamics," Europhys. Lett. **39**, 605–610 (1997).

[50] P. Español, "Fluid particle model," Phys. Rev. E **57**, 2930–2948 (1998).

[51] S. Plimpton, "Fast parallel algorithms for short-range molecular dynamics," J. Comput. Phys. **117**, 1–19 (1995).

[52] D. Einzel, P. Panzer, and M. Liu, "Boundary condition for fluid flow: Curved or rough surfaces," Phys. Rev. Lett. **64**, 2269–2272 (1990).

[53] K. Falk, F. Sedlmeier, L. Joly, R. R. Netz, and L. Bocquet, "Molecular Origin of Fast Water Transport in Carbon Nanotube Membranes: Superlubricity versus Curvature Dependent Friction," Nano Lett. **10**, 4067–4073 (2010).

[54] L. Guo, S. Chen, and M. O. Robbins, "Slip boundary conditions over curved surfaces," Phys. Rev. E **93**, 013105 (2016).

[55] D. Frenkel and B. Smit, "Understanding molecular simulation: from algorithms to applications, 2nd edition," (Elsevier, 2010) pp. 518–519.

[56] B. Dünweg and K. Kremer, "Molecular dynamics simulation of a polymer chain in solution," J. Chem. Phys. **99**, 6983–6997 (1993).

[57] S. Kämmerer, W. Kob, and R. Schilling, "Dynamics of the rotational degrees of freedom in a supercooled liquid of diatomic molecules," Phys. Rev. E **56**, 5450–5461 (1997).

[58] M. G. Mazza, N. Giovambattista, H. E. Stanley, and F. W. Starr, "Connection of translational and rotational dynamical heterogeneities with the breakdown of the Stokes-Einstein and Stokes-Einstein-Debye relations in water," Phys. Rev. E **76**, 031203 (2007).

[59] H. Hoang and G. Galliero, "Local viscosity of a fluid confined in a narrow pore," Phys. Rev. E **86**, 021202 (2012).

[60] S. Gómez-Graña, F. Hubert, F. Testard, A. Guerrero-Martínez, I. Grillo, L. M. Liz-Marzán, and O. Spalla, "Surfactant (Bi) layers on gold nanorods," Langmuir **28**, 1453–1459 (2012).

[61] J. Anderson, "Colloid Transport By Interfacial Forces," Annu. Rev. Fluid Mech. **21**, 61–99 (1989).

[62] R. P. Sear and P. B. Warren, "Diffusiophoresis in nonadsorbing polymer solutions: The Asakura-Oosawa model and stratification in drying films," Phys. Rev. E **96**, 46–48 (2017).

[63] A. J. C. Ladd, "Short-time motion of colloidal particles: Numerical simulation via a fluctuating lattice-Boltzmann equation," Phys. Rev. Lett. **70**, 1339–1342 (1993).

[64] A. Furukawa, M. Tateno, and H. Tanaka, "Physical foundation of the fluid particle dynamics method for colloid dynamics simulation," Soft Matter **14**, 3738–3747 (2018).

[65] G. Cinacchi, A. M. Pintus, and A. Tani, "Diffusion of helical particles in the screw-like nematic phase," J. Chem. Phys. **145**, 134903 (2016).

[66] D. M. Heyes, "Translational and rotational diffusion of rod shaped molecules by molecular dynamics simulations," J. Chem. Phys. **150**, 184503 (2019).

[67] X. Yang, Q. Zhu, C. Liu, W. Wang, Y. Li, F. Marchesoni, P. Hänggi, and H. P. Zhang, "Diffusion of colloidal rods in corrugated channels," Phys. Rev. E **99**, 020601 (2019).

SUPPORTING INFORMATION

1. Velocity profiles around a colloidal sphere in a flow field

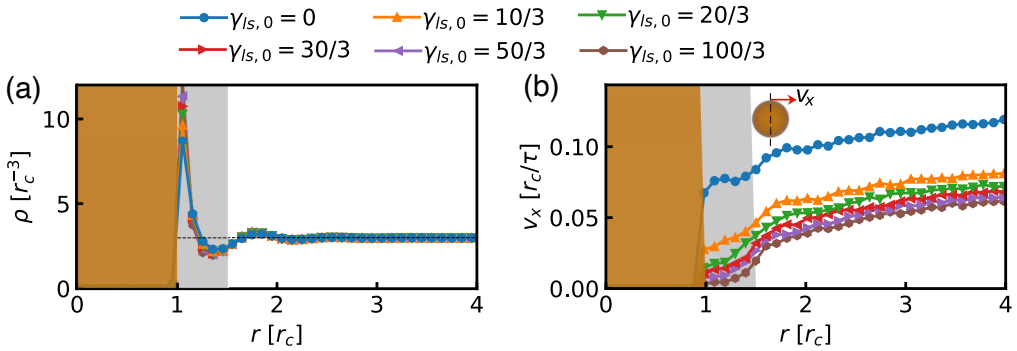

FIG. S1. The (a) density and (b) velocity profiles for the liquid particles near a solid sphere with $d = 2$ in a flow field at different values of $\gamma_{ls,0}$. The orange block represents the solid core and the grey block represents the friction shell. The simulations were performed with a cubic box of size $L_{box} = 8$ with a solid sphere fixed at the center. A constant force along $+x$ acted on all liquid particles during the simulations, resulting in a flow field with the apparent shear rate $\dot{\gamma} \sim 0.01$ (or $\ln \dot{\gamma} \sim -4.6$). In (b), v_x shows the liquid velocity perpendicular to the $y - z$ plane crossing the center-of-mass of the solid sphere as shown in the insert figure.

2. Determining the diffusion coefficient from the MSD/RMSD

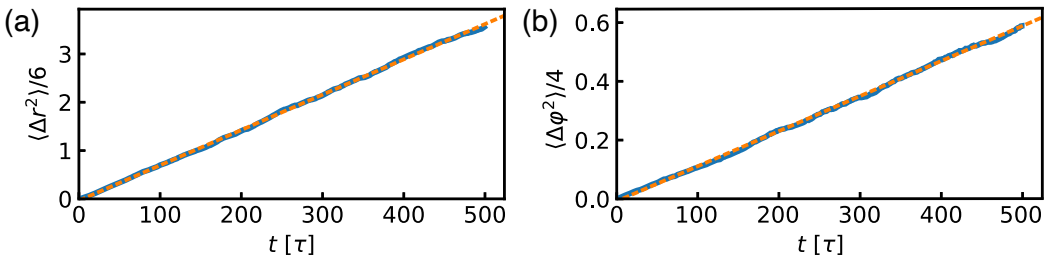

FIG. S2. Linear fitting of the (a) MSD and (b) RMSD obtained from simulations of the colloidal rod with $d = 2$ and $L = 4$ in a box of size $L_{box} = 20$ at $\gamma_{ls,0} = 20/3$. The slopes of the linear fits show the corresponding translational diffusion coefficient $D_t \sim 0.007\ r_c^2 \tau^{-1}$ and rotational diffusion coefficient $D_r \sim 0.0012\ \tau^{-1}$.

3. Size of simulation boxes

TABLE S1. Size of simulation boxes used for each colloidal particle.

shape	diameter (d)	length (L)	aspect ratio (p)	box size (L_{box})
sphere	1	1	1	4, 5, 6, 8, 12, 20
	2	1	1	4, 5, 6, 8, 12, 20
	3	1	1	5, 6, 8, 12, 20
	4	1	1	6, 8, 12, 20
	5	1	1	8, 12, 20
	6	1	1	8, 12, 20
rod	1	2	2	4, 5, 6, 8, 12, 20
	1	3	3	5, 6, 8, 12, 20
	1	4	4	6, 8, 12, 20
	1	5	5	8, 12, 20
	1	6	6	8, 12, 20
	2	4	2	6, 8, 12, 20
	2	5	2.5	8, 12, 20
	2	6	3	8, 12, 20
	3	6	2	8, 12, 20

4. Effective diameter of colloidal rods

TABLE S2. Effective diameter of the equivalent sphere for each colloidal rod.

diameter (d)	length (L)	aspect ratio (p)	effective diameter for D_t ($\overline{d}_t$)	effective diameter for D_r ($\overline{d}_r$)
1	2	2	1.58	1.77
1	3	3	1.89	2.30
1	4	4	2.18	2.82
1	5	5	2.46	3.33
1	6	6	2.73	3.83
2	4	2	3.17	3.54
2	5	2.5	3.47	4.08
2	6	3	3.78	4.61
3	6	2	4.75	5.32

5. Translational diffusion coefficients of colloidal spheres at larger surface frictions

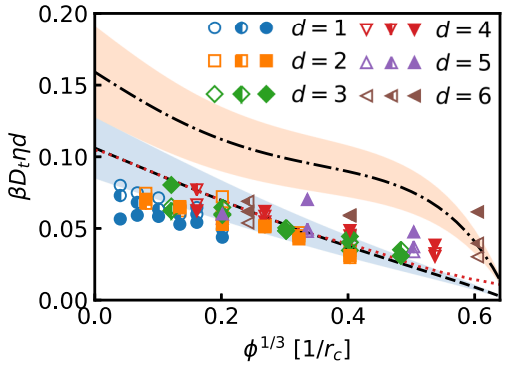

FIG. S3. Dimensionless translational diffusion coefficient ($\widetilde{D}_t$) for colloidal spheres with various values of d obtained from simulations with different box sizes at $\gamma_{ls,0} = 30/3$ (empty symbols), $\gamma_{ls,0} = 50/3$ (half-filled symbols) and $\gamma_{ls,0} = 100/3$ (solid symbols). The dash-dot (dash) line represents the results of continuum theory at slip (stick) BC obtained from Eq. 6 and 7. The colored bands show values within ±20% of the theoretical predictions.

6. Ratio of translational diffusion coefficient along the longitudinal and transverse dimensions

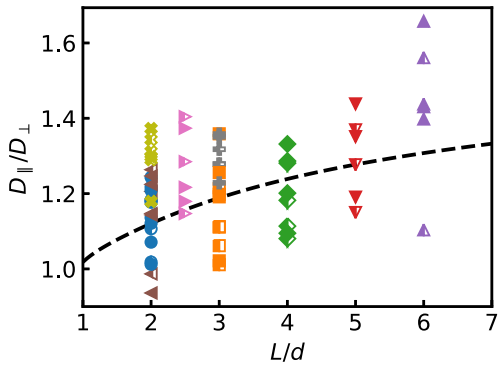

FIG. S4. Ratio of translational diffusion coefficient along the longitudinal and transverse dimensions ($D_\parallel / D_\perp$) for colloidal rods obtained from simulations at $\gamma_{ls,0} = 10/3$ (half-filled symbols) and $\gamma_{ls,0} = 20/3$ (solid symbols). The dash line is the theoretical prediction according to Eqs. 1, 2 and 5.

7. Comparison between experimental diffusion coefficients of nanorods and theoretical predictions without CTAB bilayer corrections

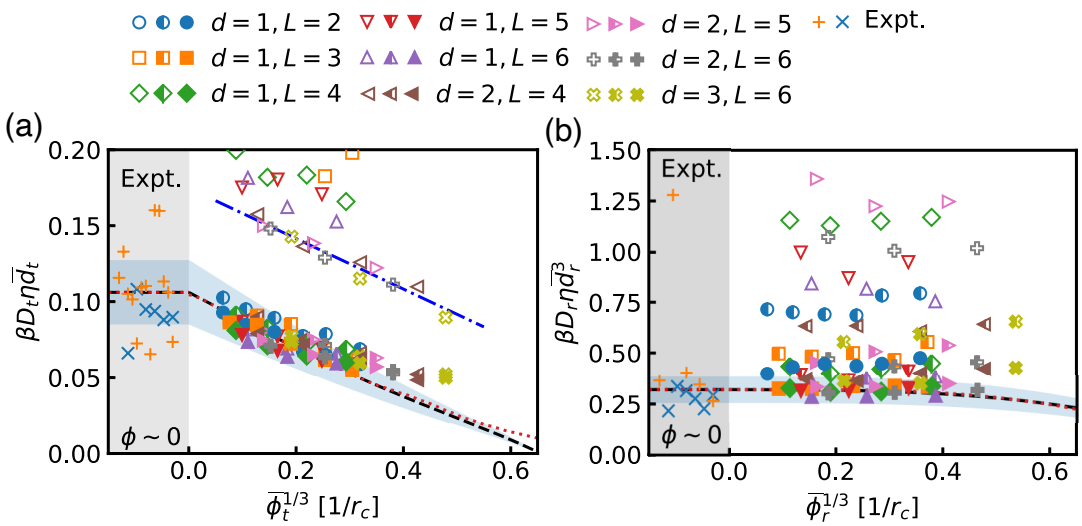

FIG. S5. The same as that of Fig. 6 in main text, except that the thickness of CTAB bilayer is not included in the effective rod dimensions when scaling the experimental data.